Available online at www.sciencedirect.com
SCIENCE DIRECT
International Journal of Mass Spectrometry 248 (2006) 47–55
International Journal of Mass Spectrometry
www.elsevier.com/locate/ijms

Photoexcitation of tetrathiafulvalene radical cations in a storage ring: Kinetics and energetics of the dissociation process

Mogens Brøndsted Nielsen [a], Thomas J.D. Jørgensen [b], James S. Forster [c], Gustav Bojesen [a], Steen Brøndsted Nielsen [d,*]

[a] *Department of Chemistry, University of Copenhagen, DK-2100 Copenhagen Ø, Denmark*
[b] *Department of Biochemistry and Molecular Biology, University of Southern Denmark, DK-5230 Odense M, Denmark*
[c] *Département de Physique, Université de Montréal, Montréal, Québec, Canada H3C3J7*
[d] *Department of Physics and Astronomy, University of Aarhus, DK-8000 Aarhus C, Denmark*

Received 1 August 2005; received in revised form 15 September 2005; accepted 19 September 2005

Abstract

In this work, we report on the dissociation kinetics of tetrathiafulvalene radical cations ($TTF^{\bullet+}$). In collisions with helium, the ions were first thermalised at room temperature or cooled to −65 °C in an ion trap before injection into an ion storage ring. Delayed dissociation of photoexcited ions was measured, and the kinetics were found to be non-trivial. The time spectrum obtained after 390 nm photoexcitation was not a single exponential decay normally observed for the dissociation of ions with a narrow energy distribution. We consider two interpretations of the time spectrum, either a multiple-exponential decay or a power-law decay. The physical implication of a multiple-exponential decay requires the presence of at least three isomers that interconvert slowly on the timescale for dissociation. In contrast, a power-law model implies a broad internal energy distribution of the excited ions. The origin of a broad distribution is, however, not obvious since we believe the width of the distribution to be narrow before excitation, about 0.1 eV, and $TTF^{\bullet+}$ is non-fluorescent. We, therefore, discard the power-law model in favour of the multiple-isomer model. The dominant dissociation reaction at low internal energies is loss of SCH as measured in collision-induced dissociation experiments and fragmentation of metastable ions. We suggest that excited $TTF^{\bullet+}$ rearranges via local minima on the potential energy surface to higher-energy isomers either before or after the photoexcitation. Isomerisation may be entropy-driven, which reduces the rate for reverse reactions to prevent equilibrium before the dissociation step. DFT calculations were applied in the search for possible structures of isomers.

Keywords: Photodissociation; Storage ring; Lifetime; Tetrathiafulvalene; Radical cation

1. Introduction

Tetrathiafulvalene, TTF (Fig. 1), is an organic sulfur-containing heterocyclic compound that has been widely exploited in both materials and supramolecular chemistry on account of its good π-donor properties [1–4]. Thus, TTF undergoes two reversible one-electron oxidations. The first oxidation leads to a 6π heteroaromatic radical cation ($TTF^{\bullet+}$), and the removal of a second electron results in the formation of a 2 × 6π heteroaromatic dication (TTF^{2+}).

In recent papers, we have studied the intrinsic properties, such as ionisation energies, of the parent TTF and related π-extended TTFs [5–7]. In particular, we investigated the outcome of high-energy collisions of $TTF^{\bullet+}$ radical cations in an accelerator mass spectrometer with different collision gases and found that TTF^{2+} was generated with high abundance when employing molecular oxygen as the collision gas [6]. Doubly charged ions were only produced in low yield by electron ionisation (EI) of TTF [8].

We next turn our attention to the dissociation kinetics of photoexcited $TTF^{\bullet+}$ ions using the unique ion storage ring technique [9,10]. An important advantage of this technique compared to others, such as Fourier transform–ion cyclotron resonance (FT-ICR) is the possibility to study the dissociation processes that take place on the microsecond to second timescale. The storage ring has been used earlier to elucidate the dissociation kinetics of several biomolecular ions, such as protonated amino acids, peptides, protein chromophores and mononucleotides [11–17]. In the present work, density functional theory (DFT) calculations

* Corresponding author.
E-mail address: sbn@phys.au.dk (S.B. Nielsen).

1387-3806/$ – see front matter © 2005 Elsevier B.V. All rights reserved.
doi:10.1016/j.ijms.2005.09.005

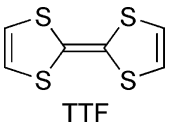

Fig. 1. Structure of tetrathiafulvalene (TTF).

are used in the interpretation of the results for $TTF^{\bullet+}$ together with collision-induced dissociation (CID) and metastable fragmentation to identify the lowest-energy dissociation channels. This part is a continuation of the work by Orduna et al. [18–21] who measured the fragmentation spectra of metastable $TTF^{\bullet+}$ and related $TTF^{\bullet+}$ radical cations from linked scan experiments.

2. Experiments

2.1. Lifetime experiments

Lifetime experiments were carried out at the electrostatic ion storage ring in Aarhus, ELISA (Fig. 2), which has been described in detail elsewhere [9,10]. TTF was dissolved in dichloromethane and electrosprayed to produce $TTF^{\bullet+}$. Ions were accumulated in a 22-pole ion trap for about 0.1 s during which time they were thermalised by collisions with helium at room temperature. In a second experiment, the trap was cooled to a temperature between −60 and −70 °C (∼208 K) by liquid nitrogen. After extraction from the trap, the ions were accelerated to a translational kinetic energy of 22 keV. A magnet was used to select the $TTF^{\bullet+}$ ions (m/z 204) that were subsequently injected into the storage ring. The pressure in the ring was a few times 10^{-11} mbar which limited the storage time of the ions to a few seconds. Metastable decay and collisions with residual gas led to the production of neutral fragments that were counted by a microchannel plate (MCP) detector if they were formed in the injection side of the ring (Fig. 2).

After about 50 ms of storage time, the ions were irradiated by a laser pulse from either a Nd:YAG laser (Quanta-Ray, Spectra-Physics) or a pulsed alexandrite laser (PAL101 from LightAge, Somerset, New Jersey). A delay of 50 ms ensured that all metastable ions formed during the injection process had decayed. The fundamental output of the Nd:YAG laser, 1064 nm, was frequency doubled to 532 nm which was again doubled to 266 nm. The output of the PAL laser was set to 780 nm, and this light was frequency doubled to 390 nm. Delayed dissociation of the photoexcited ions was again measured in the MCP detector.

Unfortunately, our experiment does not provide any information on the dissociation channel and whether the dissociation channel varies with time. All neutrals that hit the detector were measured.

2.2. Low-energy collision-induced dissociation experiments

To help identify the dissociation channels, low-energy collision-induced dissociation spectra were acquired using a quadrupole-time-of-flight (Q-TOF 1) mass spectrometer (Micromass, Manchester, UK) equipped with an electrospray ion source. A dichloromethane solution of TTF was sprayed (10 μL/min) from a steel capillary held at 3 kV toward a skimmer cone at 40 V. The source block temperature was 80 °C, and the precursor ions were mass selected by the quadrupole and then accelerated into the hexapole collision cell at several laboratory collision energies (10–25 eV). Argon was used as a collision gas at an indicated manifold pressure of 8.5×10^{-5} mbar (the pressure was not measured directly in the CID collision chamber), and center-of-mass collision energies ranged from 1.6 to 4.1 eV. The product ions were mass analysed by an orthogonal TOF analyser.

2.3. MIKE experiments

In mass-analysed ion kinetic energy (MIKE) experiments, $TTF^{\bullet+}$ ions were formed by electron ionisation of vaporised TTF and accelerated to a kinetic energy of 10 keV. Measurements were carried out with a JEOL JMS-HX110/HX four-sector instrument with the $E_1B_1E_2B_2$ geometry (E: electrostatic sector and B: magnetic sector). The $TTF^{\bullet+}$ parent ions were selected by the E_1B_1 sectors and fragments formed in the third field-free region from metastable ions were monitored by E_2.

2.4. Laser desorption experiments

Positive ion laser desorption mass spectra were recorded with a Perseptive Voyager STR time-of-flight mass spectrometer operating in reflectron mode. Two microliters of a

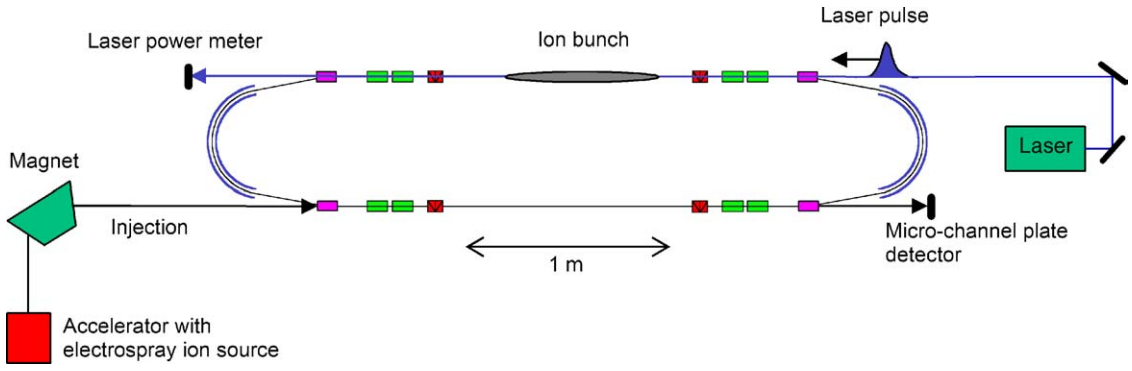

Fig. 2. Layout of the electrostatic ion storage ring ELISA, showing ion injection and detection of neutrals by a microchannel plate detector at one side of the ring and a laser for excitation of the stored ions at the other side.

dichloromethane solution of TTF were applied to the target plate. The solvent was evaporated and the procedure repeated until a thin layer of TTF crystals had formed on the plate. A nitrogen laser (337 nm, 5 ns pulse width) was used to desorb and ionise the sample. The acceleration voltage was 20 kV. Spectra were averaged over 200 shots.

3. Theoretical details

Molecular geometries were optimised at the B3LYP/6-31+G(d) level with the Gaussian98 and 03 program packages [22]. Frequencies were calculated to verify that the calculated structures are local minima on the potential energy surface and to correct for zero-point kinetic energies. Finally, single-point energy calculations were performed at the B3LYP/6-311++G(2d,p) level.

4. Results and discussion

4.1. Lifetime measurements

Time spectra for the decay of 390 nm photoexcited $TTF^{\bullet+}$ radical cations are shown in Fig. 3. Although the initial temperature of the ions was either room temperature (300 K) or between −60 and −70 °C (∼208 K), the time spectra are quite similar. The revolution time of the ions in ELISA is 57.6 μs which is the spacing between the points.

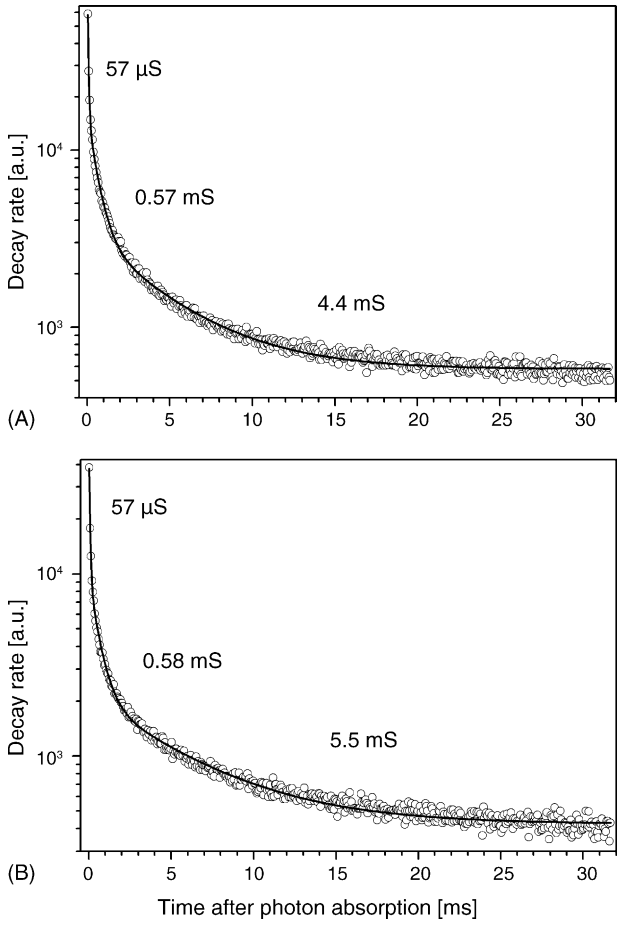

Fig. 3. Decay of $TTF^{\bullet+}$ after 390 nm photon absorption. The ions were irradiated after 50 ms of storage, and their initial temperature was either 300 K (A) or 208 K (B). The revolution time of the ions is 57.6 μs which is the spacing of the points. At least three exponentials are needed to fit the data.

To understand these decays, we will assume a model that has been used successfully to describe the decay rate of ions in ELISA [11–17] and another storage ring, ASTRID (the Aarhus Storage Ring Denmark) [23].

4.2. Statistical decay rate

An important parameter for the decay of the $TTF^{\bullet+}$ ions is their internal energy E, which we can evaluate by assuming that thermal equilibrium was established in the 22-pole ion trap. The average internal energy before absorption of a photon is calculated from the vibrational frequencies ω_i,

$$\langle E\rangle = \sum_i \frac{\hbar\omega_i}{\exp(\hbar\omega_i/k_B T_c) - 1}, \quad (1)$$

where $\hbar$ is the Plancks constant, k_B the Boltzmanns constant, T_c the canonical temperature of the ion ensemble and i runs over all vibrational degrees of freedom. At 208 and 300 K, $\langle E\rangle$ is 0.085 and 0.184 eV, respectively.

The energy distributions are shown in Fig. 4. The number of states was counted by a modified Beyer–Swinehart algorithm from the vibrational frequencies [24,25] and multiplied by the Boltzmann factor at each internal energy. Fits to the cumulative distributions provided Gaussian representations,

$$g(E) = \frac{1}{\sqrt{2\pi\sigma^2}} \exp\left(-\frac{(E - E_{max})^2}{2\sigma^2}\right), \quad (2)$$

where the maxima of the distributions, E_{max}, are at 0.050 and 0.157 eV and the widths σ are 0.076 and 0.114 eV at the two temperatures. In a simpler approach that works well for large molecules, the maximum is approximated by the average energy and the width is calculated from $\sigma = (C_c k_B)^{1/2} T_c$ [26]. C_c is the canonical heat capacity and is easily calculated from the vibra-

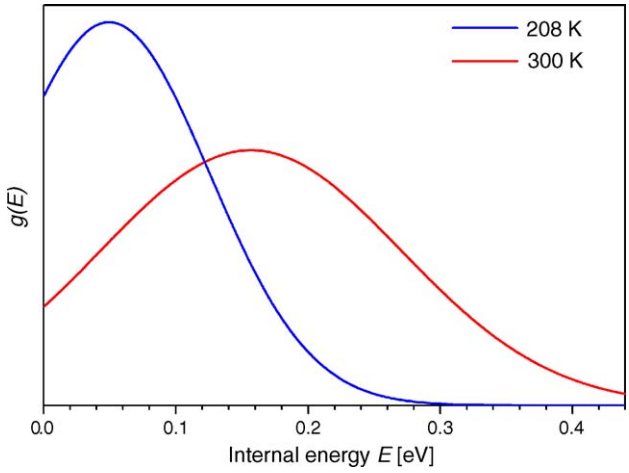

Fig. 4. Approximate internal energy distributions of $TTF^{\bullet+}$ ions at 208 and 300 K.

tional frequencies,

$$C_c = k_B \sum_i \left(\frac{\hbar\omega_i}{k_B T_c}\right)^2 \frac{\exp(-\hbar\omega_i)}{(1-\exp(-\hbar\omega_i/k_B T_c))^2} \quad (3)$$

At initial temperatures of 208 and 300 K, the heat capacities are 8.66×10^{-4} and 1.273×10^{-4} eV/K, and the widths are 0.057 and 0.099 eV, respectively. The agreement is fairly good with the more exact analysis. After photoabsorption, the energy distributions are moved up in energy by the photon energy but the widths are unchanged (see discussion later). This implies a shift from a canonical ensemble to a microcanonical one.

For an isolated system, it was previously shown that an Arrhenius-like expression can be used for the rate constant,

$$k(E) = A \exp\left(\frac{-E_0}{k_B(T - E_0/2C - E_0^2/(12C^2T))}\right) \quad (4)$$

where A is a preexponential factor, E_0 the activation energy, T the microcanonical temperature before the decay and C is the microcanonical heat capacity at energy $E - E_0/2$ [27–29]. C is obtained from the canonical heat capacity, $C - C_c(s-1)/s$, where s is the number of vibrational degrees of freedom. The microcanonical temperature is defined in terms of the level density $\rho(E)$ by $1/k_B T = \mathrm{d}\ln\rho/\mathrm{d}E$. The $E_0/2C + {E_0}^2/(12C^2T)$ correction to the effective temperature is the finite-heat-bath correction obtained from a Taylor expansion to second order at the energy $E - E_0/2$. We stress that this approach is based on a microcanonical rate constant, which is necessary since a canonical temperature is not valid after photon absorption (the width of the distribution is unchanged after photon absorption). An alternative way of analysing the data would be by RRKM theory.

To summarize, for a specific internal energy, the decay rate decreases exponentially with a characteristic time constant. However, the spread in internal energies results in a tail on the exponential decay. The decay rate at time t can be expressed as,

$$I(t) = \int \mathrm{d}E k(E) g(E) \exp\{-k(E)t\} \quad (5)$$

For an ensemble with a broad internal energy distribution, the time dependence of the decay rate is determined by depletion of the hottest molecules. It was earlier demonstrated that the decay rate in this case follows a power-law t^n with a power close to $n = -1$ [29]. Thus, there is no characteristic time, and the decay rate is a strongly increasing function of microcanonical temperature. The decay may be quenched by radiative cooling, which leads to an exponential cut-off of the $1/t$ decay at a characteristic quenching time [29]. In earlier experiments, characteristic cooling times for collisionally activated amino acids were found to be ca. 10 ms [11].

Within this work, we have two different ion temperatures, and in the following, we will examine whether the initial temperature of the ions may change during the storage prior to laser excitation. It is well known that isolated ions in a chamber reach thermal equilibrium after some time from the absorption of blackbody radiation and their emission of radiation from IR active modes. The rate of absorption of blackbody radiation is obtained from the Einstein B coefficient and the Planck radiation spectrum $\Phi(\omega)$,

$$k_{abs} = \sum_i B(\omega_i)\Phi(\omega_i) \quad (6)$$

$$B(\omega_i) = \frac{{\mu_i}^2}{6\varepsilon_0\hbar^2} = \frac{{q_i}^2}{6\varepsilon_0\hbar\omega_i M_i} \quad (7)$$

$$\Phi(\omega) = \frac{2\hbar\omega^3}{\pi c^3} \frac{1}{\exp(\hbar\omega/k_B T_w) - 1} \quad (8)$$

where μ_i is the transition dipole moment of the IR active mode i, q_i and M_i the dipole derivative and reduced mass, respectively, of the vibration and T_w is the temperature of the walls (room temperature). IR intensities, q_i^2/M_i, and vibrational frequencies, ω_i, were obtained from the DFT calculation for $TTF^{\bullet+}$. IR intensities were used unscaled whereas frequencies were scaled by 0.9614 to account for anharmonicity [30]. The time constant for the absorption of an IR photon was found to be 1 s which is more than one order of magnitude greater than the timescale of the experiment, that is, the storage time of 50 ms before the laser pulse is fired. Hence, IR absorption is neglected.

Let us now return to Fig. 3. Clearly, one exponential does not satisfactorily describe the data. The width in the internal energy distribution gives a tail to a simple exponential decay according to Eq. (5) but this is still not sufficient, cf. Fig. 5 where three fits are shown with Arrhenius parameters (A, E_0) of (10^{10} s^{-1}, 1.90 eV), (10^{13} s^{-1}, 2.45 eV) and (10^{16} s^{-1}, 2.90 eV). The rate constants are not varying enough within the microcanonical temperature distribution (Fig. 6) unless the A factor becomes unphysically high (10^{30} s^{-1}). We therefore discuss two other interpretations, a multiple-exponential decay and power-law decay.

4.3. Multiple-exponential decay

To fit the data, at least three exponentials are needed with time constants of 57 μs, 0.58 and 4–5 ms (Fig. 3). The collisions with residual gas will give decays with time constants in the order of

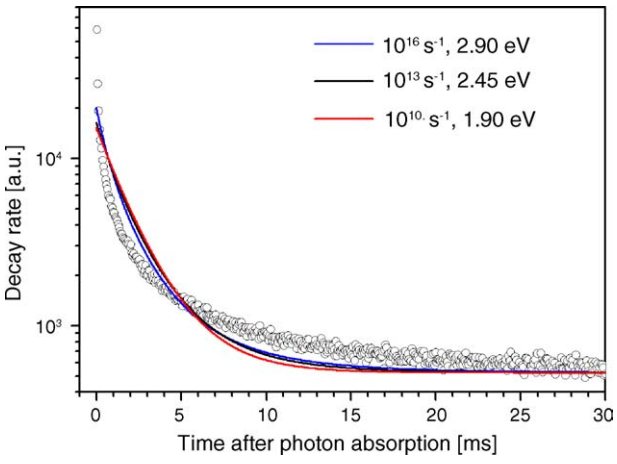

Fig. 5. Fits to the decay spectrum shown in Fig. 3 with three sets of Arrhenius parameters A and E_0. The decay rates are calculated from Eq. (5).

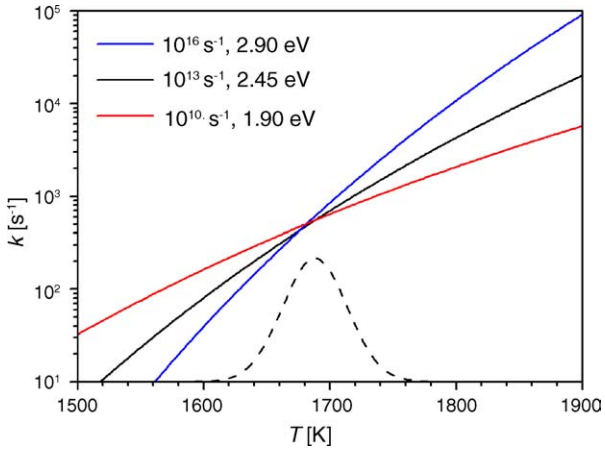

Fig. 6. Rate constants calculated from Eq. (4) used to calculate the decay rates shown in Fig. 5. The dashed curve shows the microcanonical temperature distribution after 390 nm photon absorption.

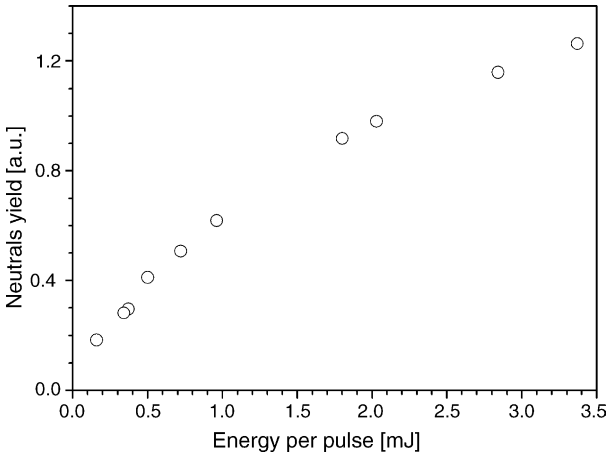

Fig. 8. Neutrals yield as a function of the pulse energy. At low pulse energies, the dependence is linear.

seconds, and thus, all of the decay is due to photoexcitation. The relative fractions of the three components differ slightly at the two temperatures in favour of the long-lived component at the lower temperature. At 300 K initial temperature, the fractions are 0.17, 0.30 and 0.53 and at 208 K, 0.16, 0.27 and 0.57 for increasing time constants.

More than one exponential is necessary if the decay is the result of a different number of photons absorbed. However, a power dependence study reveals that all of the decay is due to the same number of photons absorbed (Fig. 7) and, in addition, that we are dealing with one-photon absorption (Fig. 8). The increase of the neutrals signal with laser-pulse energy is linear for small energies and reaches a saturation limit when all ions in the bunch have absorbed at least one photon. Hence, we conclude that any ions that have absorbed two photons dissociate too quickly to survive to the other side of the ring (travel time of 28 μs).

In this analysis, three exponentials and one-photon absorption imply that the beam contains at least three isomers which dissociate faster than their time for interconversion. Each isomer fragments in a statistical manner but equilibrium between the isomers is not established before dissociation. Otherwise the decay would be characterised by a single decay rate. The rate of interconversion could be unfavoured because of large entropy changes. Isomers are either formed already in the ion source or immediately after photoexcitation.

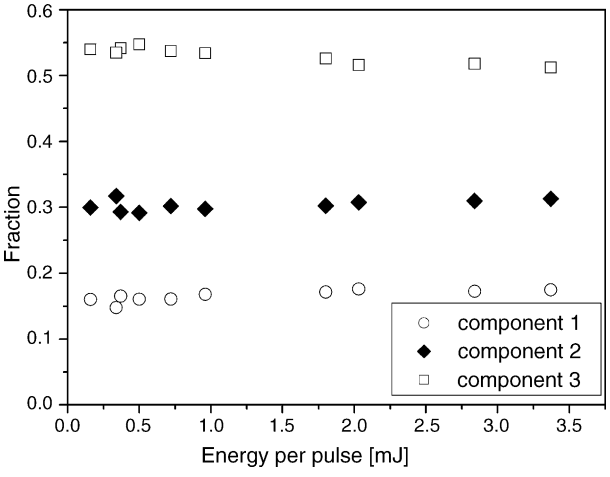

Fig. 7. Fractions of each of the components of the three-exponential fit as a function of pulse energy. The constant fractions indicate that all of the decay is due to the same number of photons absorbed.

Multiexponential decay would also be observed if a fraction of the electronically excited ions crossed from the excited doublet surface to quartet surfaces instead of internal conversion to the doublet ground state surface. Electronic quartet states act as bottlenecks for the dissociation reaction because of the spin-forbidden intersystem crossing to the doublet ground state. A similar interpretation was previously used to explain the two-exponential decay of photoexcited porphyrin ions [14,15]. In that case, one lifetime was assumed to be the statistical lifetime for dissociation and the other the result of trapping in a triplet state before crossing to the electronic ground state and dissociation. The population of two long-lived electronic quartet states of $TTF^{\bullet+}$ seems very unlikely and has, to our knowledge, not been reported in the literature.

4.4. Power-law decay

There could however be another explanation for the decay based instead on statistical dissociation. Multiple-exponential fits often occur when the energy distribution of the ions is broad. In this situation, the spectra are fitted by the function [11],

$$I(t) = N\left(\frac{t}{\tau}\right)^{\delta} \frac{1}{\exp(t/\tau) - 1} + K \tag{9}$$

where N is a normalisation factor and the factor $(t/\tau)^{\delta}$ corrects the effective power in the power-law t^n at short times ($t < \tau$) to $n = -1 + \delta$, while the additive constant K accounts for fragmentation by collisions in the ring. τ is the time constant for quenching of the internal energy by IR radiative emission. When $\delta = 0$, the function reduces to a $1/t$ decay which applies for the decay of ions for which the internal energy distribution is broad enough to give a large spread in lifetimes, that is, the rate constant changes significantly over the internal energy distribution.

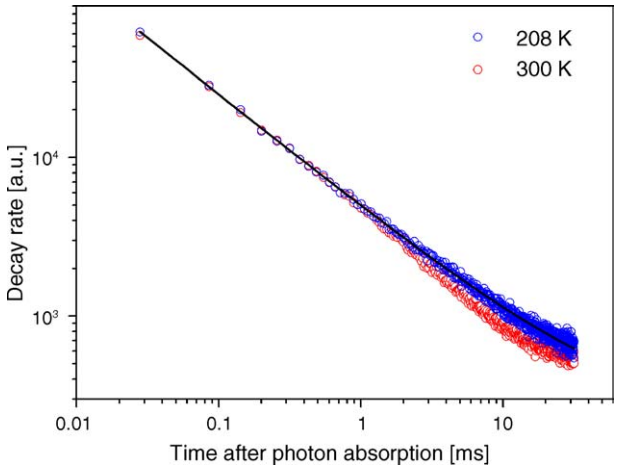

Fig. 9. The data in Fig. 3 is represented in a log–log plot. The red and blue circles are associated with decay of $TTF^{\bullet+}$ ions at 300 and 208 K, respectively, before laser excitation. The solid black line is a fit to the function $N_0 t^{-0.71} + K$. After 2 ms, the "red" signal is quenched.

For a power-law decay, plotting $I(t)$ versus t on a log–log plot should give a straight line. Indeed, this is the case as shown in Fig. 9. In other words, if this model is valid for the decay of $TTF^{\bullet+}$ ions, the width of the internal energy distribution contributes to the observed decay. Such a power-law fit gives a power of $n = -0.71$.

There are at least two explanations for a deviation in the power from $n = -1$. First of all, the energy distribution is obviously not flat (Fig. 4). When we sample the decay of ions from the high-energy side of the maximum, n is numerically less than 1 since the number of ions increases with decreasing energy. In contrast, if we sample the decay of ions from the low-energy side of the distribution, n is numerically larger than 1 since the number of ions decreases with energy. Thus, the curve appears either less steep or steeper than that for a t^{-1} decay. Competing reaction channels also reduce n numerically. As the energy distribution depletes from the high-energy side, other dissociation channels may take over, and the decay is less steep than the case when only one channel is open over the whole energy range.

The decay from the excitation of ions at room temperature is quenched after a time of ca. 2 ms, which could be due to radiative cooling. A fit using Eq. (9) provides a time constant of 5 ms. The total rate constant for infrared radiation from vibrations was calculated from [11],

$$k_{\mathrm{rad}} = \sum_i \frac{2\omega_i {q_i}^2}{3M_i c^3} \tag{10}$$

Again using the calculated IR intensities and IR frequencies and assuming all vibrations are populated, we find a rate constant of 165 s^{-1} and the reciprocal is the lifetime for deexcitation by radiation being 6 ms. This calculated radiative lifetime is in fine agreement with the measured 5 ms time constant.

There is however another explanation for the quenching that would better account for the difference between ions with initial temperatures of 300 and 208 K. After about 2 ms, the decay may be governed by the low-energy side of the energy distribution. As argued above, the power here is numerically larger than 1. At the initial temperature of 208 K, the maximum of the energy distribution is at a lower internal energy and hence the transition to steeper power-law decay occurs at a later time.

4.5. Excitation by ultraviolet light

In a similar experiment, we irradiated $TTF^{\bullet+}$ ions at room temperature with 266 nm photons to raise the initial internal energy distribution by 4.67 eV. Again one exponential function was not sufficient and two were required with time constants of 23 μs and 0.18 ms (Fig. 10A). In this analysis, the time constants are for dissociation channels via two different isomers that do not interconvert on the timescale of the dissociation.

In Fig. 10B, the data from 266 nm excitation are plotted as a log–log plot to investigate the other approach for the decay. The difference in energy between 390 and 266 nm photons is 1.47 eV, which is greater than the width of the internal energy distribution. The high internal energy after photoabsorption implies that we only observe the decay of ions from the low-energy tail of the internal energy distribution since ions with higher internal energy do not survive half a revolution in the ring. Indeed, a power-law fit results in a power of $n = -1.28$ in agreement with this interpretation. In this model, at 390 nm excitation, the observed depletion of ions results from those sampled at the

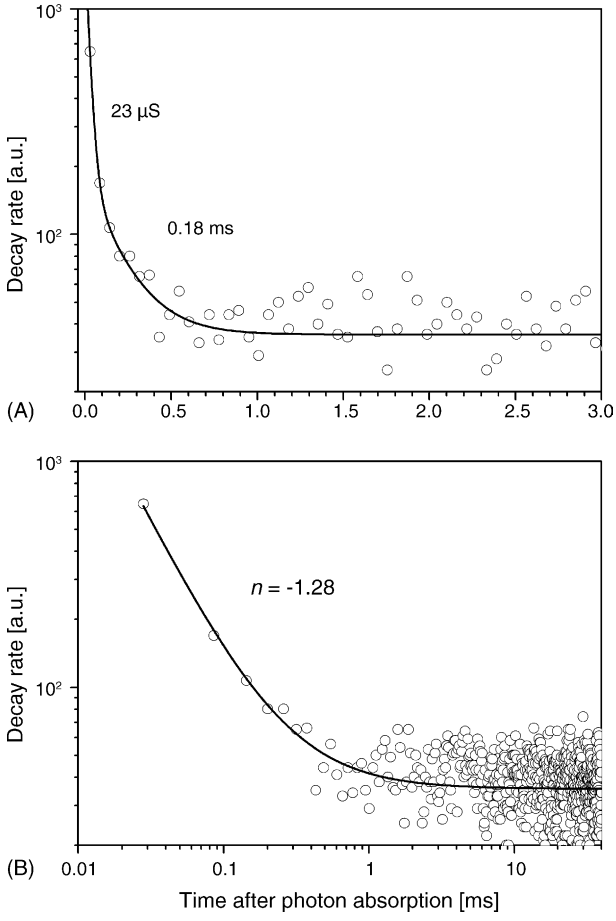

Fig. 10. Decay of 266 nm photoexcited $TTF^{\bullet+}$ radical cations: (A) two-exponential fit to the data and (B) the solid line in the log–log plot is a fit to the function $N_0 t^{-1.28} + K$.

high-energy side of the energy distribution ($n = -0.71$), whereas at 266 nm excitation, the observed depletion of ions is from the low-energy side ($n = -1.28$).

4.6. Possible origins of a broad internal energy distribution

So far, we have neglected the origin of a broad internal energy distribution which is required for the statistical power-law model. The initial width of the internal energy distribution is not sufficient to give a power-law decay, and we therefore need to consider other possibilities for a broad internal energy distribution after photon absorption.

First, there is the possibility for fluorescence since photons with different energies are emitted from the ensemble of ions determined by the Franck-Condon factors. Fluorescence studies of $TTF^{\bullet+}$ both in solution and in low-temperature organic glasses have previously been reported [31,32]. In solution, no fluorescence was observed [31], whereas a slight fluorescence was observed in the glass [32]. The fluorescence quantum yield in the glass was not determined but is expected to be even lower than that of the 4,4′-dimethyl-5,5′-diphenyltetrathiafulvalene radical cation (5×10^{-3}) [31]. We, therefore, conclude that fluorescence does not contribute to our measured decay from delayed dissociation. In addition, the internal energy of the ions would most likely be too low after photon emission to cause dissociation. According to calculations discussed later in the paper, at least 1.2 eV of the internal energy is required for dissociation.

Another possibility could be prompt hydrogen loss after excitation since $[TTF - H]^+$ ions (m/z 203) have high enough translational kinetic energies to be stored in the ring (22 keV × 203/204). This loss was previously assumed to be the explanation for a power-law decay of protonated tryptophan after ultraviolet photoexcitation [12]. Recently, Tseng et al. [33] measured the kinetic energy release distribution for H loss from photoexcited phenol to be broad with a width of about 0.6 eV, and the ions energy distribution is therefore broadened by 0.6 eV. The H elimination process occurs on a repulsive surface. However, calculations indicate that the H-loss channel in the case of $TTF^{\bullet+}$ is too energetic and there would be no energy left for further dissociation. Moreover, hydrogen loss is a very minor channel from the MIKE and CID experiments as well as laser desorption experiments (vide infra).

The simplicity of the power-law model seems very attractive but there is no apparent physical or chemical explanation for a broadening of the internal energy distribution after photon absorption. We, therefore, consider the non-equilibrium model for dissociation to be a more probable explanation for the data, and that the ions undergo isomerisation to higher-energy isomers that are not in equilibrium with each other. Each channel has a unique dissociation rate, and the overall result is a multi-exponential decay.

4.7. Reaction channels

In the following, we elucidate the reaction channels based on CID, metastable fragmentation and quantum chemical calculations.

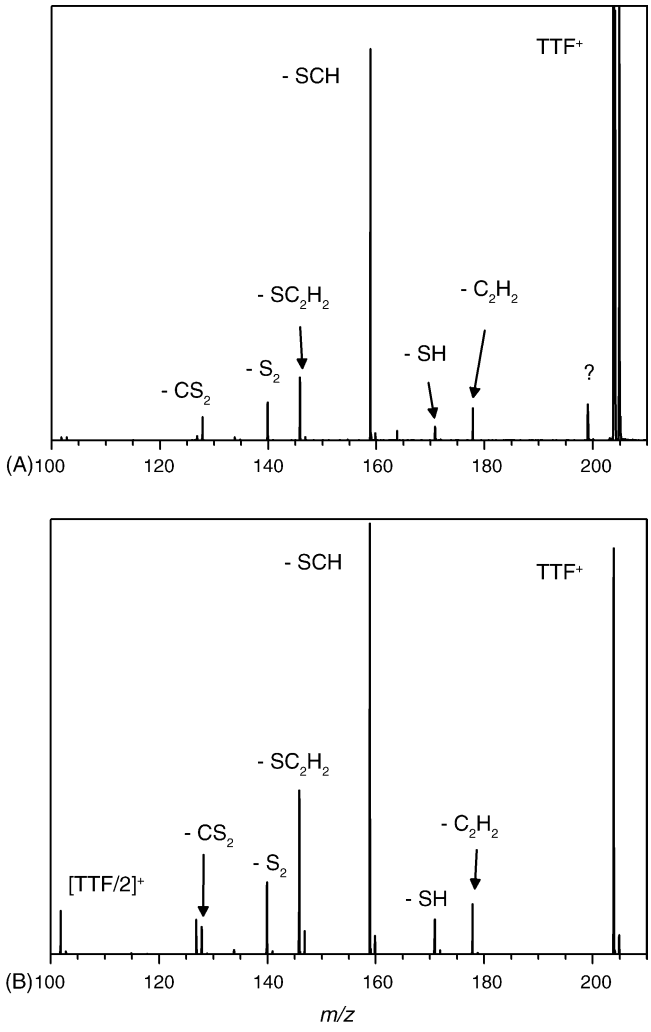

Fig. 11. Low-energy CID spectrum of $TTF^{\bullet+}$. The center-of-mass collision energies are: 1.6 eV (A) and 4.1 eV (B).

The CID spectrum of $TTF^{\bullet+}$ at 1.6 eV center-of-mass collision energy is shown in Fig. 11A. The major fragmentation channel is loss of SCH which results in the peak at m/z 159. Minor peaks correspond to ions formed after loss of CS_2 (m/z 128), S_2 (m/z 140), SC_2H_2 (m/z 146), SH (m/z 171) and C_2H_2 (m/z 178). At higher ion beam energies, peaks at m/z 102 (symmetric cleavage of fulvalene bond) and m/z 127 (loss of CS_2H) appear in the CID spectrum (Fig. 11B).

The MIKE spectrum of $TTF^{\bullet+}$ shown in Fig. 12 is, not surprisingly, similar to previously reported metastable fragmentation spectra recorded in the linked scan mode. Moreover the spectrum is very similar to the low-energy CID spectrum. It does not matter whether cold ions from the electrospray ion source are heated in collisions with helium or hot ions are formed directly from the electron ionisation process. The major peak is again at m/z 159 (Fig. 12) (the kinetic energy release for this channel is 26 meV). Furthermore, Garín et al. [21] found that the fragmentation spectrum of metastable tetrathianaphthalene ions (an isomer of $TTF^{\bullet+}$, see structure **3** in Table 1) is similar to that of $TTF^{\bullet+}$ and it displays the same intense signal at m/z 159. All in all, the observations lend strong

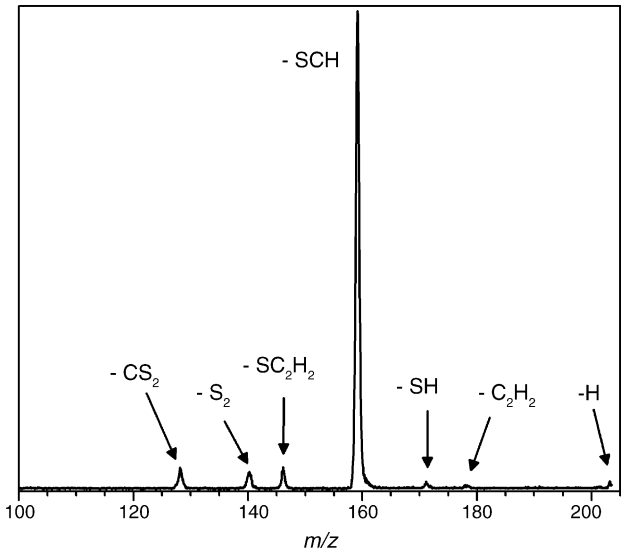

Fig. 12. MIKE spectrum of metastable $TTF^{\bullet+}$.

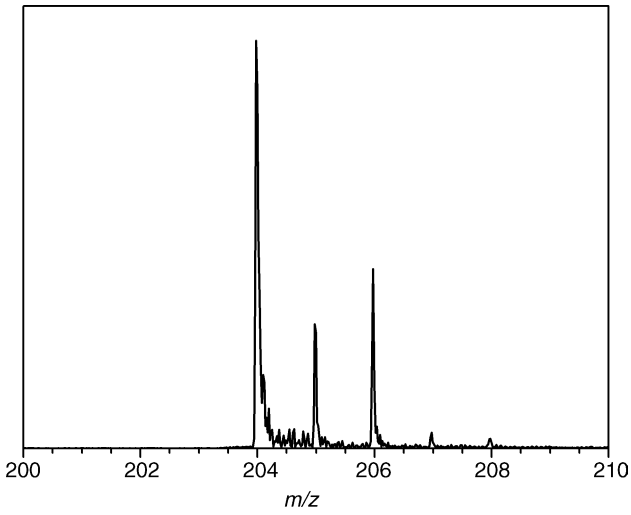

Fig. 13. Laser desorption mass spectrum of crystallised TTF.

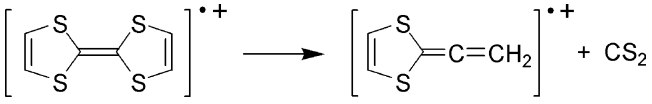

Fig. 14. The lowest-energy channel for fragmentation of $TTF^{\bullet+}$.

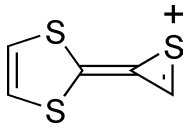

Fig. 15. The thiirane fragment ion formed after loss of SCH.

support to the formation of isomers of $TTF^{\bullet+}$ ions prior to dissociation.

It is difficult to determine the internal energy of the metastable ions or collisionally activated ions. The center-of-mass collision energy ranges from 1.6 to 4.1 eV but this is the maximum energy transferred in the collision process. Comparisons to high-energy collisions are therefore useful. Earlier we reported 50 keV collision-induced dissociation spectra of $TTF^{\bullet+}$ and found that the highest peak corresponds to loss of SC_2H_2. Losses of C_2H_2 and SCH were also observed in addition to symmetric cleavage of the fulvalene bond. Several ions of lower masses were detected, e.g., SCH^+, C_2S^+, C_2HS^+, C_3HS^+, $C_3H_2S^+$, CS_2^+, $C_2S_2^+$ and $C_2S_2H^+$ [6]. The formation of these ions requires larger energies as revealed from the calculations below.

Based on these experiments, hydrogen loss from vibrationally excited $TTF^{\bullet+}$ is irrelevant. Unfortunately, we do not have the equipment to record the photodissociation fragment spectra. Instead, we carried out a laser desorption (LD) experiment using 337 nm light. Fig. 13 shows a LD spectrum in the region of the *m*/*z* 204 ion. This spectrum agrees with the interpretation that hydrogen loss does not take place since there is no indication of a peak at *m*/*z* 203. At the high photon flux, the *m*/*z* 204 peak is in saturation, and therefore, the isotope pattern appears to be wrong.

Model calculations were carried out to determine the reaction energies for H loss, SCH loss and other channels. Direct hydrogen loss from $TTF^{\bullet+}$ is too costly, 4.63 eV, to be of importance. Hence, we conclude that H loss followed by dissociation is unlikely for $TTF^{\bullet+}$. Loss of C_2H_2, SC_2H_2 or S_2 from $TTF^{\bullet+}$ requires about 3 eV and are possible reactions after the absorption of a 3.2 eV photon but likely occur with a rate too low to matter in the limited timescale of our experiment. Loss of CS_2 from $TTF^{\bullet+}$ and formation of the fragment ion shown in Fig. 14 only needs 1.19 eV and is the most favourable reaction but again this process cannot occur by a simple dissociation.

From the CID and MIKE experiments, the dominant reaction channel is SCH loss, which is in agreement with previously reported mass spectral data. The fragmentation has been suggested to produce the thiirane product depicted in Fig. 15 [8,19]. However, from our calculations its formation can be neglected since it requires 5.2 eV.

It seems that one or more rearrangement reactions are necessary to bring the reaction energy within the allowed internal energy interval and to give SCH loss. Hence, calculations were made for different isomers of $TTF^{\bullet+}$ that may be formed after photoexcitation or already in the ion source (Table 1). Two isomers that are less than 1 eV more energetic than $TTF^{\bullet+}$ were found, and these may play a significant role for the dissociation kinetics. It is likely that many more isomers exist.

Table 1
Relative energies (eV) of three isomers of the TTF radical cation

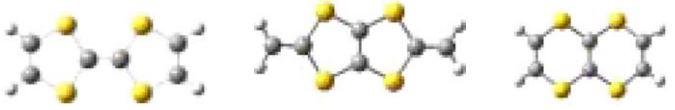

1 $TTF^{\bullet+}$ (0) **2** (0.78) **3** (0.96)

5. Concluding remarks

We have found that the decay of $TTF^{\bullet+}$ radical cations after absorption of a single photon, 390 or 266 nm is not just a simple

exponential but instead a multiple-exponential decay or power-law decay. Based on fragmentation experiments and model calculations, rearrangement reactions take place prior to dissociation, and it is argued that dissociation occurs from high-energy isomers that interconvert slowly (non-equilibrium situation).

The present work contributes to the complicated description of the behaviour of organic molecular ions after photoexcitation, which have been the subject of several recent studies applying the same technique. We have earlier found that protonated tripeptides, such as Tyr–Trp–TyrH$^+$, after absorption of UV light exhibited an exponential decay, and from decay spectra acquired at different photon energies Arrhenius parameters could be deduced [12]. Delayed dissociation of porphyrin anion and cations has been measured due to trapping in triplet states after intersystem crossing from an excited singlet state to a lower-lying triplet state [14,15]. A further example is UV-photoexcited protonated tryptophan ions that lose hydrogen while in an electronically excited state, and subsequent dissociation of the tryptophan radical cations follows a $1/t$ decay [12]. Competition between non-statistical and statistical dissociation was also found for adenosine 5′-monophosphate cations and anions after absorption of 266 nm photons [13]. Our study provides a new case since, as we have shown, TTF$^{\bullet+}$ radical cations undergo an unexpected $1/t$ or multiexponential decay after photoexcitation, and this is likely due to isomerisation processes.

Acknowledgements

We acknowledge many fruitful discussions with Jens Ulrik Andersen and Preben Hvelplund. Katrine Petersen is thanked for assistance on the MIKE experiments. SBN and MBN acknowledge support from the Danish Natural Science Research Council (Grants Nos. 21-02-0129 and 2111-04-0018).

References

[1] M.R. Bryce, Adv. Mater. 11 (1999) 11.
[2] M. Brøndsted Nielsen, C. Lomholt, J. Becher, Chem. Soc. Rev. 29 (2000) 153.
[3] M.R. Bryce, J. Mater. Chem. 10 (2000) 589.
[4] J.L. Segura, N. Martín, Angew. Chem. Int. Ed. 40 (2001) 1372.
[5] S. Brøndsted Nielsen, M. Brøndsted Nielsen, New J. Chem. 25 (2001) 769.
[6] S. Brøndsted Nielsen, M. Brøndsted Nielsen, H.J.Aa. Jensen, Phys. Chem. Chem. Phys. 5 (2003) 1376.
[7] K. Qvortrup, M.T. Jakobsen, J.-P. Gisselbrecht, C. Boudon, F. Jensen, S. Brøndsted Nielsen, M. Brøndsted Nielsen, J. Mater. Chem. 14 (2004) 1768.
[8] J.R. Andersen, H. Egsgaard, E. Larsen, K. Bechgaard, E.M. Engler, Org. Mass Spectrom. 13 (1978) 121.
[9] S.P. Møller, Nucl. Instrum. Methods Phys. Res. Sect. A 394 (1997) 281.
[10] J.U. Andersen, P. Hvelplund, S. Brøndsted Nielsen, S. Tomita, H. Wahlgreen, S.P. Møller, U.V. Pedersen, J.S. Forster, T.J.D. Jørgensen, Rev. Sci. Instrum. 73 (2002) 1284.
[11] J.U. Andersen, H. Cederquist, J.S. Forster, B.A. Huber, P. Hvelplund, J. Jensen, B. Liu, B. Manil, L. Maunoury, S. Brøndsted Nielsen, U.V. Pedersen, H.T. Schmidt, S. Tomita, H. Zettergren, Eur. Phys. J. D 25 (2003) 139.
[12] J.U. Andersen, H. Cederquist, J.S. Forster, B.A. Huber, P. Hvelplund, J. Jensen, B. Liu, B. Manil, L. Maunoury, S. Brøndsted Nielsen, U.V. Pedersen, J. Rangama, H.T. Schmidt, S. Tomita, H. Zettergren, Phys. Chem. Chem. Phys. 6 (2004) 2676.
[13] S. Brøndsted Nielsen, J.U. Andersen, J.S. Forster, P. Hvelplund, B. Liu, U.V. Pedersen, S. Tomita, Phys. Rev. Lett. 91 (2003) 048302.
[14] M.R. Calvo, J.U. Andersen, P. Hvelplund, S. Brøndsted Nielsen, U.V. Pedersen, J. Rangama, S. Tomita, J. Chem. Phys. 120 (2004) 5067.
[15] C.B. Nielsen, J.S. Forster, P.R. Ogilby, S. Brøndsted Nielsen, J. Phys. Chem. A 109 (2005) 3875.
[16] L.H. Andersen, H. Bluhme, S. Boyé, T.J.D. Jørgensen, H. Krogh, I.B. Nielsen, S. Brøndsted Nielsen, U.V. Pedersen, A. Svendsen, Phys. Chem. Chem. Phys. 6 (2004) 2617.
[17] S. Brøndsted Nielsen, J.U. Andersen, P. Hvelplund, B. Liu, S. Tomita, J. Phys. B At. Mol. Opt. Phys. 37 (2004) R25 (review).
[18] J. Orduna, J. Garín, Rapid Commun. Mass Spectrom. 11 (1997) 590.
[19] C. Rovira, J. Tarrés, M. Dias, J. Garín, J. Orduna, Rapid Commun. Mass Spectrom. 9 (1995) 276.
[20] J. Orduna, J. Garín, P. Frère, T.-T. Nguyen, A. Gorgues, L. Sánchez, N. Martín, C. Seoane, Rapid Commun. Mass Spectrom. 9 (1995) 856.
[21] J. Garín, J. Orduna, J.M. Royo, A.-M. Le Quéré, H. Müller, Rapid Commun. Mass Spectrom. 17 (2003) 547.
[22] Gaussian 98, Revision A.9., M.J. Frisch, G.W. Trucks, H.B. Schlegel, G.E. Scuseria, M.A. Robb, J.R. Cheeseman, et al., Gaussian Inc., Pittsburgh, PA, 1998;
Gaussian 03, Revision B.03, M.J. Frisch G.W. Trucks, H.B. Schlegel, G.E. Scuseria, M.A. Robb, J.R. Cheeseman, et al., Gaussian Inc., Pittsburgh, PA, 2003.
[23] J.U. Andersen, C. Brink, P. Hvelplund, M.O. Larsson, B. Bech Nielsen, H. Shen, Phys. Rev. Lett. 77 (1996) 3991.
[24] T.S. Beyer, D.F. Swinehart, Commun. Assoc. Machines 16 (1973) 379.
[25] G. Bojesen, unpublished results.
[26] J.U. Andersen, E. Bonderup, K. Hansen, J. Chem. Phys. 114 (2001) 6518.
[27] J.U. Andersen, E. Bonderup, K. Hansen, J. Phys. B At. Mol. Opt. Phys. 35 (2002) R1.
[28] C.E. Klots, J. Chem. Phys. 90 (1989) 4470.
[29] K. Hansen, J.U. Andersen, P. Hvelplund, S.P. Møller, U.V. Pedersen, V.V. Petrunin, Phys. Rev. Lett. 87 (2001) 123401.
[30] A.P. Scott, L. Radom, J. Phys. Chem. 100 (1996) 16502.
[31] P.R. Ashton, V. Balzani, J. Becher, A. Credi, M.C.T. Fyfe, G. Mattersteig, S. Menzer, M. Brøndsted Nielsen, F.M. Raymo, J.F. Stoddart, M. Venturi, D.J. Williams, J. Am. Chem. Soc. 121 (1999) 3951.
[32] K. Zimmer, B. Gödicke, M. Hoppmeier, H. Meyer, A. Schweig, Chem. Phys. 248 (1999) 263.
[33] C.-M. Tseng, Y.T. Lee, C.-K. Ni, J. Chem. Phys. 121 (2004) 2459.